THE JOURNAL OF CHEMICAL PHYSICS **134**, 114502 (2011)

Thermodynamics of *d*-dimensional hard sphere fluids confined to micropores

Hyungjun Kim,[1,2,a)] William A. Goddard III,[1,2] Kyeong Hwan Han,[3] Changho Kim,[3] Eok Kyun Lee,[3] Peter Talkner,[4] and Peter Hänggi[4]
[1]*Center for Materials Simulations and Design, Graduate School of EEWS (WCU), Korea Advanced Institute of Science and Technology, Daejeon 305-701, South Korea*
[2]*Materials and Process Simulation Center (MC 139-74), California Institute of Technology, Pasadena, California 91125, USA*
[3]*Department of Chemistry and School of Molecular Science (BK21), Korea Advanced Institute of Science and Technology, Daejeon 305-701, South Korea*
[4]*Institut Physik, Universität Augsburg, D-86135 Augsburg, Germany*

(Received 8 November 2010; accepted 20 February 2011; published online 15 March 2011)

We derive an analytical expression of the second virial coefficient of d-dimensional hard sphere fluids confined to slit pores by applying Speedy and Reiss' interpretation of cavity space. We confirm that this coefficient is identical to the one obtained from the Mayer cluster expansion up to second order with respect to fugacity. The key step of both approaches is to evaluate either the surface area or the volume of the d-dimensional exclusion sphere confined to a slit pore. We, further, present an analytical form of thermodynamic functions such as entropy and pressure tensor as a function of the size of the slit pore. Molecular dynamics simulations are performed for $d = 2$ and $d = 3$, and the results are compared with analytically obtained equations of state. They agree satisfactorily in the low density regime, and, for given density, the agreement of the results becomes excellent as the width of the slit pore gets smaller, because the higher order virial coefficients become unimportant. © *2011 American Institute of Physics*. [doi:10.1063/1.3564917]

I. INTRODUCTION

The understanding of thermodynamic behaviors of fluids in restricted geometries has been of long-standing interest. Owing to the recent rapid development of nanotechnology, quantitative observations and characterizations have become available for a number of interesting thermodynamic properties of fluid systems with strong geometric confinement. Furthermore, confined fluids have a wide range of applications such as biological[1] and artificial[2,3] microchannels, carbon nanotubes,[4] nanoporous catalysts,[5,6] molecular sieves,[7,8] and molecularly imprinted materials.[9] Specifically, the establishment of theoretical foundations of thermodynamics and transport properties of confined fluids[10] is critical for the further development of current technology to solve the energy problems; for example, the underlying principles of hydrogen gas absorption in templated porous materials, such as metal-organic frameworks and covalent organic frameworks,[11–15] or ionic transport through proton exchange membrane fuel cells,[16–23] are governed by the physics of confined fluids.

The quest for fundamental understanding of confined fluids has invoked a number of theoretical approaches and numerical simulation studies.[24–30] Most analytical studies with the goal to derive an analytical equation of state (EOS) of confined fluids are based on hard sphere (HS) systems interacting with hard walls (HW) with idealized geometries such as slit and cylindrical pores. In order to obtain more accurate analytical EOS of fluids confined in such shapes of pores, various mathematical techniques have been employed; for example, the transfer matrix method by Xin *et al.*,[24] the pore-bulk distribution coefficient calculated by Glandt,[25] the low-dimensional technique used by Post and Kofke,[26] and the transfer operator method by Kamenetskiy *et al.*[27] However, a simple and accurate analytical EOS covering a wide range of pore sizes and fluid densities has not been developed yet.

Recently, Mukamel and Posch formulated a method to calculate thermodynamic properties of hard disks confined in a two-dimensional channel.[28] They derived an analytical form of the free energy of confined hard disks, which is exact up to second virial terms, by employing the Mayer cluster expansion method. Then, by taking appropriate derivatives of the free energy with respect to the channel length and width, they were able to obtain each component of the anisotropic pressure tensor in the low density region and for the whole range of pore sizes.

For bulk HS fluids, which belong to the most extensively studied thermodynamic systems,[31–36] various statistical thermodynamic problems have been successfully reduced to statistical geometric problems in terms of a "free volume" approach.[33–36] Employing the free volume approach, a pictorial representation of a thermodynamic problem becomes possible and concepts like temperature, energy, and motion are effectively eliminated. The concept of the free volume is defined as the available space for a given particle when all neighbor particles are frozen. Hoover and his co-workers have succeeded in deriving the EOS of d-dimensional HS fluids as a function of the volume $\langle V_f \rangle$ and the surface area $\langle S_f \rangle$ of the free volume.[33,34] Speedy and Reiss modified this

---

[a)] Electronic mail: linus16@kaist.ac.kr.

Downloaded 16 Mar 2011 to 137.250.81.221. Redistribution subject to AIP license or copyright; see http://jcp.aip.org/about/rights_and_permissions

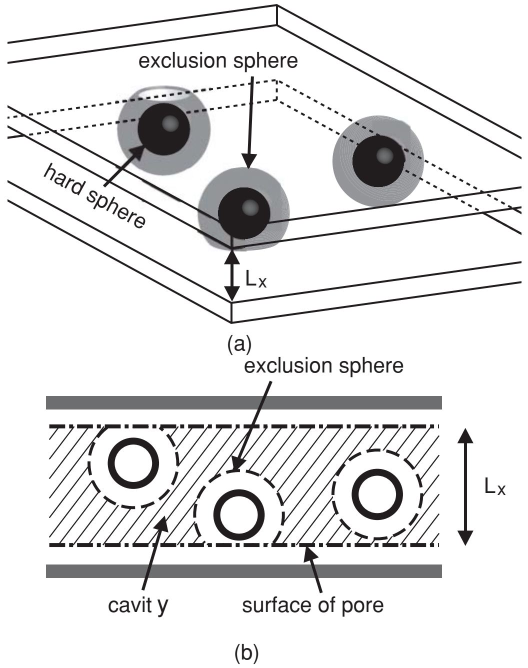

FIG. 1. Schematic diagram of the cavity space. The solid spheres represent HS particles and the dashed spheres indicate the exclusion spheres of the respective HS. In the lower panel, a 2d-cut of the slit pore perpendicular to the walls indicated by thick dark gray lines is sketched; the cavity space is shown as shaded region.

relationship by introducing another geometrical quantity, known as the cavity, which is defined as the available space for the addition of one more particle.[35,36] The EOS of the d-dimensional fluid of HS with diameter σ can be expressed in terms of the ensemble-averaged cavity volume $\langle V_c \rangle$ and the ensemble-averaged surface area $\langle S_c \rangle$:

$$\frac{Pv}{k_B T} = 1 + \frac{\sigma}{2d} \frac{\langle S_c \rangle}{\langle V_c \rangle}, \tag{1}$$

where P, v, and T denote pressure, volume per particle, and temperature, respectively. The validity of Eq. (1) for bulk HS systems has been tested and verified for a broad range of densities by directly evaluating the surface area and the volume of the cavity using the Voronoi tessellation method.[37,38]

The conjunction of Eq. (1) with the virial theorem tells that the interparticle virial is proportional to the surface area of the cavity normalized with respect to the volume of the cavity. If the particles move in a confined space, the interparticle virial is suppressed by the confined geometry. Thus, the size of the cavity volume has to be modified depending on the confining geometry.

The present paper is organized as follows. In Sec. II, we start with the definitions of the cavity volume and the surface area of the d-dimensional HS system confined to a slit-shaped pore composed of two parallel $(d-1)$-dimensional hyperplanes. Then, we derive the EOS and thermodynamic functions valid up to the second virial term using the cavity volume and surface area. Next we derive the second virial coefficient, B_2 for the same system using Mayer's cluster expansion,[28] and confirm that the two approaches produce identical result. In Sec. III, we examine the validity of our equation of state by comparing with numerical simulation results for $d = 2$ and $d = 3$ dimensional HS fluid systems confined to a slit pore, and discuss the contribution of the second virial term to the thermodynamics of confined HS fluids. Concluding remarks follow in Sec. IV.

II. GENERAL FORMULATION

A. The second virial coefficient of confined fluids: Free volume approach

We consider a system composed of N d-dimensional spherical particles with mass m in a confined space at temperature T. These particles interact with each other via the hard sphere potential:

$$u(r) = \begin{cases} \infty, & r < \sigma \\ 0, & \text{otherwise} \end{cases}, \tag{2}$$

where r denotes the distance between the centers of two HS particles.

The motion of the particles is confined to the space provided by the slit-shaped pore composed of two parallel $(d-1)$-dimensional hyperplanes. We choose the normal direction of the hyperplane as x-direction. If we consider a HW interaction potential of the form

$$u_w(x) = \begin{cases} \infty, & |x| > L_x/2 \\ 0, & \text{otherwise} \end{cases}, \tag{3}$$

the motion of the center of the HS in the x-direction is restricted to the interval $[-L_x/2, L_x/2]$. Here the actual pore width is $L_x + 2\sigma$. However, the total available volume for a given particle inside of the slit pore is defined as a product of the surface area of the slit pore and L_x. Thus, we call L_x the free width.

The shaded region in Fig. 1(b) depicts the cavity space of the confined HS fluid system. It is to be noted that the contribution to the surface area of the cavity space in the case of the confined system is not only from the *exclusion spheres* of the HS particles [dashed lines in Fig. 1(b)], but also from the surface area of the pore [dashed-dotted lines in Fig. 1(b)], but the contribution to the interparticle virial comes from the former part, only. Therefore, Eq. (1) which is valid for bulk fluid system has to be modified as follows: (1) define the surface area of the cavity space only contributed from the exclusion sphere of each particle, and (2) determine the volume of the cavity space in a confined geometry, which is defined as the total available volume of the slit pore minus the union of the exclusion spheres of all particles within the pore. Denoting the surface area per particle according to definition (1) by S_{ExS} and the volume per particle of the union of exclusion spheres by V_{ExS}, we can rewrite Eq. (1) as

$$\frac{Pv}{k_B T} = 1 + \frac{\sigma}{2d} \frac{\langle S_{\mathrm{ExS}} \rangle}{v - \langle V_{\mathrm{ExS}} \rangle}, \tag{4}$$

where the angular brackets denote the ensemble average over all possible configurations in the confined space, and v is the specific volume defined as the total volume of the confined space divided by N.

Generally, at finite densities there are always some overlaps of the exclusion spheres. Thus, the computations of

Downloaded 16 Mar 2011 to 137.250.81.221. Redistribution subject to AIP license or copyright; see http://jcp.aip.org/about/rights_and_permissions

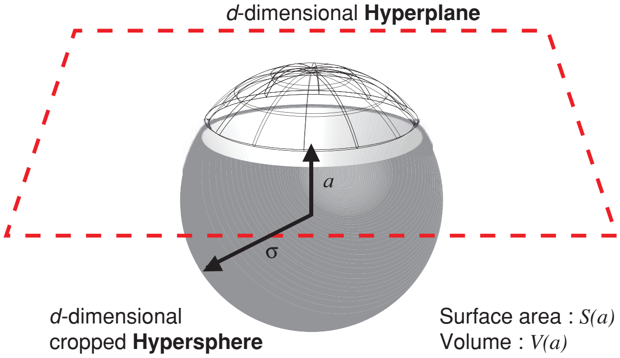

FIG. 2. In the d-dimensional space, the hypersphere with radius σ is defined by $x^2 + y^2 + z^2 + \cdots = \sigma^2$. A hyperplane located at $x = a$ divides the hypersphere into two trimmed hyperspheres, where $a \in [0, \sigma]$. We refer to the larger one of the two as to the cropped hypersphere. The surface area and the volume of the cropped hypersphere (mathematically, defined as $\{\vec{r}; |\vec{r}| < \sigma \text{ and } \vec{r} \cdot \hat{x} < a\}$) are denoted by $S(a)$ and $V(a)$, respectively, each of which is determined by the surface area and volume of the corresponding exclusion sphere. Explicit expressions are given in Eqs. (12)–(25).

$\langle S_{\mathrm{ExS}} \rangle$ and $\langle V_{\mathrm{ExS}} \rangle$ require a numerical approach. However if we assume that the density of the system is sufficiently low, then we can consider the contribution from the two-body interaction only, and the resulting EOS is valid up to the second virial term. This case corresponds to the situation without any overlap of the exclusion spheres. The perturbation expansion of the denominator of Eq. (4) up to second order then leads to

$$\frac{Pv}{k_B T} = 1 + \frac{\sigma}{2d} \frac{\langle S_{\mathrm{ExS}} \rangle}{v} + O\left(\frac{1}{v^2}\right) \tag{5}$$

and the second virial coefficient B_2 can be expressed in terms of $\langle S_{\mathrm{ExS}} \rangle$ as

$$B_2 = \frac{\sigma}{2d} \langle S_{\mathrm{ExS}} \rangle . \tag{6}$$

For the bulk fluid, the surface of nonoverlapping exclusion spheres S_{ExS} is given by the surface areas of d-dimensional hyperspheres of radius σ, $S^{\mathrm{HS}} = (2\pi^{d/2}\sigma^{d-1})/\Gamma(d/2)$. Accordingly, the second virial coefficient of d-dimensional HS bulk system can be obtained from Eq. (6) as, $B_2^{\mathrm{HS}}(d) = (\sqrt{\pi}\sigma)^d/[d\Gamma(d/2)]$.

If the fluid is confined to the slit-shaped pore, the invariance with respect to translations in the x-direction is broken, and the exclusion sphere of a given particle depends on the x-coordinate of the particle because a part of the exclusion sphere can be trimmed by a pore wall as depicted in Fig. 1. We denote the x-directional position dependent surface area of the exclusion sphere by $S_{\mathrm{ExS}}(x)$. Assuming that the probability distribution of the particles is uniform along the x-direction, which is an appropriate approximation in the low density regime, the ensemble average of $S_{\mathrm{ExS}}(x)$ reduces to an average with respect to the x-coordinate:

$$\langle S_{\mathrm{ExS}} \rangle = \frac{1}{L_x} \int_{-L_x/2}^{L_x/2} S_{\mathrm{ExS}}(x)\, dx. \tag{7}$$

In order to calculate $S_{\mathrm{ExS}}(x)$, we consider a hypersphere with radius σ and a hyperplane bisecting the hypersphere (see Fig. 2). The surface area of the larger part, i.e., of the *cropped sphere* which is denoted by $S(a)$, depends on the distance a of the sphere from the wall. Then, $S_{\mathrm{ExS}}(x)$ can be expressed in terms of $S(a)$ as

$S_{\mathrm{ExS}}(x) =$

1. when $L_x \geq 2\sigma$,

$$\begin{cases} S\left(\frac{L_x}{2} - x\right), & \frac{\tilde{L}_x}{2} < x < \frac{L_x}{2} \\ S(\sigma), & -\frac{\tilde{L}_x}{2} \leq x \leq \frac{\tilde{L}_x}{2} \\ S\left(\frac{L_x}{2} + x\right), & -\frac{L_x}{2} < x < -\frac{\tilde{L}_x}{2} \end{cases}, \tag{8}$$

2. when $\sigma \leq L_x < 2\sigma$,

$$\begin{cases} S\left(\frac{L_x}{2} - x\right), & -\frac{\tilde{L}_x}{2} < x < \frac{L_x}{2} \\ S\left(\frac{L_x}{2} - x\right) + S\left(\frac{L_x}{2} + x\right) - S(\sigma), & \frac{\tilde{L}_x}{2} \leq x \leq -\frac{\tilde{L}_x}{2}, \\ S\left(\frac{L_x}{2} + x\right), & -\frac{L_x}{2} < x < \frac{\tilde{L}_x}{2} \end{cases} \tag{9}$$

and

3. when $0 < L_x < \sigma$,

$$S\left(\frac{L_x}{2} - x\right) + S\left(\frac{L_x}{2} + x\right) - S(\sigma), \tag{10}$$

where $\tilde{L}_x = L_x - 2\sigma$. The substitution of Eqs. (8)–(11) into Eq. (7) leads to

$\langle S_{\mathrm{ExS}} \rangle =$

$$\begin{cases} \frac{2}{L_x} \int_0^{L_x} S(a)\, da - S(\sigma), & 0 < L_x < \sigma \\ \frac{2}{L_x} \int_0^{\sigma} S(a)\, da + \left(1 - \frac{2\sigma}{L_x}\right) S(\sigma), & L_x \geq \sigma \end{cases}, \tag{11}$$

where $S(\sigma) = S^{\mathrm{HS}}$.

The integral giving $S(a)$ can be evaluated in the hyperspherical coordinate system (details are shown in Appendix A):

$$S(a) = C \frac{d(d-1)}{\sigma^2} \left[F^{(\mathrm{I})}(1) + \frac{a}{\sigma} F^{(\mathrm{I})}\left(\frac{a^2}{\sigma^2}\right) \right], \tag{12}$$

where

$$C = \frac{\pi^{(d-1)/2} \sigma^{d+1}}{\Gamma((d+1)/2)\, d} \tag{13}$$

and

$$F^{(\mathrm{I})}(x) = {}_2F_1\left(\frac{1}{2}, \frac{3-d}{2}, \frac{3}{2}; x\right), \tag{14}$$

being a Gauss hypergeometric function.

Substituting Eq. (12) into Eqs. (6) and (11), we obtain

$$B_2 = \frac{C}{L_x} \left[\frac{L_x}{\sigma} F^{(\mathrm{II})}(1) - 1 \right], \tag{15}$$

Downloaded 16 Mar 2011 to 137.250.81.221. Redistribution subject to AIP license or copyright; see http://jcp.aip.org/about/rights_and_permissions

if $L_x \geq \sigma$, and otherwise,

$$B_2 = \frac{C}{L_x}\left[F^{(\mathrm{II})}\left(\frac{L_x^2}{\sigma^2}\right) - 1\right], \tag{16}$$

where

$$F^{(\mathrm{II})}(x) = {}_2F_1\left(-\frac{1}{2}, \frac{1-d}{2}, \frac{1}{2}; x\right). \tag{17}$$

In a recent work, Mukamel and Posch expressed the second virial coefficient B_2 of confined hard disks ($d = 2$) in terms of the Mayer function.[28] We generalize this relation to the d-dimensional system:

$$B_2 = -\frac{q(L_x)}{2} + \frac{L_x}{2d}\frac{dq(L_x)}{dL_x}, \tag{18}$$

where

$$q(L_x) = -\int 1 - e^{-\beta u(r_{12})} d^d r_{12}, \tag{19}$$

which can be simplified to

$$q(L_x) = -\int_\Omega d^d r_{12}, \tag{20}$$

for the HS interaction, where Ω is the d-dimensional sphere satisfying $r_{12} = |\vec{r}_1 - \vec{r}_2| \leq \sigma$, $\vec{r}_i$ being the position of i'th particle.

In the case of confined fluids, the component of the particle position transversal to the confining walls is restricted to $x \in [-L_x/2, L_x/2]$. This confinement transforms the geometrical shape of Ω into the cropped exclusion sphere proposed above. Thus, $\int_\Omega d^d r_{12}$ corresponds to the ensemble-averaged volume of cropped exclusion spheres, $\langle V_{\mathrm{ExS}}\rangle$, which leads to

$$q(L_x) = -\langle V_{\mathrm{ExS}}\rangle. \tag{21}$$

Then Eq. (18) becomes

$$B_2 = \frac{\langle V_{\mathrm{ExS}}\rangle}{2} - \frac{L_x}{2d}\frac{d\langle V_{\mathrm{ExS}}\rangle}{dL_x}, \tag{22}$$

where the ensemble average of $V_{\mathrm{ExS}}(x)$ can be obtained by performing an average with respect to x [refer Eq. (7)]:

$$\langle V_{\mathrm{ExS}}\rangle = \frac{1}{L_x}\int_{-L_x/2}^{L_x/2} V_{\mathrm{ExS}}(x)\,dx. \tag{23}$$

The calculation procedure of $\langle V_{\mathrm{ExS}}\rangle$ is closely parallel to the procedure by which $\langle S_{\mathrm{ExS}}\rangle$ is calculated following Eqs. (8)–(11). The ensemble-averaged exclusion volume $\langle V_{\mathrm{ExS}}\rangle$ can be expressed in terms of the volume $V(a)$ of the hypersphere with radius σ cropped by a hyperplane at distance a from the center of the hypersphere as (see Fig. 2)

$$\langle V_{\mathrm{ExS}}\rangle = \begin{cases} \dfrac{2}{L_x}\displaystyle\int_0^{L_x} V(a)\,da - V(\sigma), & 0 < L_x < \sigma \\ \dfrac{2}{L_x}\displaystyle\int_0^{\sigma} V(a)\,da + \left(1 - \dfrac{2\sigma}{L_x}\right)V(\sigma), & L_x \geq \sigma \end{cases}. \tag{24}$$

The volume of the d-dimensional "cropped hypersphere" $V(a)$ is (see Appendix A),

$$V(a) = C\frac{(d-1)}{\sigma}\left[F^{(\mathrm{I})}(1) + \frac{a}{\sigma}F^{(\mathrm{I})}\left(\frac{a^2}{\sigma^2}\right) + A\right], \tag{25}$$

where

$$A = \frac{a(\sigma^2 - a^2)^{\frac{d-1}{2}}}{\sigma^d(d-1)}. \tag{26}$$

Substitution of Eq. (25) into Eqs. (22)–(24) yields exactly the same result for the B_2 as those shown in Eqs. (15) and (16), which are obtained using the free volume idea. This comparison confirms that for d-dimensional HS fluids confined to the slit-shaped pore, Speedy's and Reiss' EOS, which is based on the free volume approach, agrees with the EOS achieved by Mayer's cluster expansion at least up to the second virial term.

Furthermore, we note that this equivalence still holds for the HS fluids that is confined to a channel satisfying periodic boundary conditions (PBC) in the x-direction, which is one of the systems proposed by Mukamel and Posch (see Appendix B).[28]

B. Free energy and pressure tensor components

Knowing the analytical form of B_2 we are able to derive other thermodynamic quantities of HS fluids confined to a slit pore.

For example, the diagonal components of the pressure tensor $P_{\alpha\alpha}$ can be obtained by differentiating the specific free energy $f = F/N$ with respect to L_α:

$$P_{\alpha\alpha}v = -L_\alpha\frac{\partial f}{\partial L_\alpha}, \tag{27}$$

where $\alpha \in \{x, y, z, \cdots\}$. Since the thermodynamic pressure is a sum of the diagonal components of the pressure tensor $P = \sum_\alpha P_{\alpha\alpha}/d$, Eqs. (5)–(27) lead to

$$1 + \frac{\sigma}{2d}\frac{\langle S_{\mathrm{ExS}}\rangle}{v} = -\frac{1}{dk_BT}\sum_\alpha L_\alpha\frac{\partial f}{\partial L_\alpha}. \tag{28}$$

Recalling the specific free energy of the bulk system obtained up to the second order virial expansion is given by

$$\frac{f}{k_BT} = \frac{f^{\mathrm{ideal}}}{k_BT} + \frac{B_2^{\mathrm{HS}}}{v}, \tag{29}$$

we assume the solution form of the differential equation Eq. (28) as

$$\frac{f}{k_BT} = \frac{f^{\mathrm{ideal}}}{k_BT} + \frac{g(L_x)}{v}, \tag{30}$$

where $g(L_x)/v$ is the excess free energy contributed by the second virial term and

$$\frac{f^{\mathrm{ideal}}}{k_BT} = -1 - \ln v + d\ln\lambda. \tag{31}$$

Here λ is the thermal de Broglie wavelength, $h/\sqrt{2\pi mk_BT}$.

Then, Eq. (28) is simplified as

$$\frac{\sigma}{2d}\langle S_{\mathrm{ExS}}\rangle = g(L_x) - \frac{L_x}{d}\frac{\partial g(L_x)}{\partial L_x}, \tag{32}$$

Downloaded 16 Mar 2011 to 137.250.81.221. Redistribution subject to AIP license or copyright; see http://jcp.aip.org/about/rights_and_permissions

whose formal solution is given as

$$g\left(L_x\right) = -\frac{\sigma\left(L_x\right)^d}{2}\int\frac{\langle S_{\mathrm{ExS}}\rangle}{\left(L_x\right)^{d+1}}dL_x. \tag{33}$$

From Eq. (33), we obtain f, and, by means of Eq. (27) the leading terms of the diagonal elements of the pressure tensor, P_{xx} and $P_{\mu\mu}$ with $\mu\in\{y,z,\cdots\}$, become

if $L_x\geq\sigma$

$$\frac{f}{k_BT} = \frac{f^{\mathrm{ideal}}}{k_BT}+\frac{C}{vL_x}\left[\frac{L_x}{\sigma}F^{(\mathrm{II})}\left(1\right)-\frac{d}{d+1}\right],$$

$$\frac{P_{xx}v}{k_BT} = 1+\frac{C}{vL_x}\left[\frac{L_x}{\sigma}F^{(\mathrm{II})}\left(1\right)-\frac{2d}{d+1}\right], \tag{34}$$

and

$$\frac{P_{\mu\mu}v}{k_BT} = 1+\frac{C}{vL_x}\left[\frac{L_x}{\sigma}F^{(\mathrm{II})}\left(1\right)-\frac{d}{d+1}\right], \tag{35}$$

where C as in Eq. (13).

If $0\leq L_x<\sigma$

$$\frac{f}{k_BT} = \frac{f^{\mathrm{ideal}}}{k_BT}+\frac{C}{vL_x}\left[F^{(\mathrm{II})}\left(\frac{L_x^2}{\sigma^2}\right)-\frac{d}{d+1}-D\right],$$

$$\frac{P_{xx}v}{k_BT} = 1+\frac{C}{vL_x}\left[F^{(\mathrm{II})}\left(\frac{L_x^2}{\sigma^2}\right)-\frac{2d}{d+1}+D\left(d-1\right)\right], \tag{36}$$

$$\frac{P_{\mu\mu}v}{k_BT} = 1+\frac{C}{vL_x}\left[F^{(\mathrm{II})}\left(\frac{L_x^2}{\sigma^2}\right)-\frac{d}{d+1}+D\right], \tag{37}$$

where

$$D = \frac{\left(\sigma^2-L_x^2\right)^{\frac{d+1}{2}}}{\sigma^{d+1}\left(d+1\right)}. \tag{38}$$

C. Asymptotic behavior of pressure in the limit of wide and narrow slits

The thermodynamic behavior of the HS fluid system confined to the slit pore is expected to approach that of bulk d-dimensional HS fluids as L_x goes to infinity. On the other hand, the behavior of the same system is expected to converge to that of a $(d-1)$-dimensional bulk HS as L_x approaches 0. Here we show that the components of the pressure tensor exhibit the expected behavior.

In the limit $L_x\to\infty$, both Eqs. (34)–(35) approach the bulk value of pressure, i.e.:

$$\lim_{L_x\to\infty}\frac{P_{xx}\left(L_x\right)v}{k_BT} = 1+\frac{B_2^{\mathrm{HS}}\left(d\right)}{v}, \tag{39}$$

$$\lim_{L_x\to\infty}\frac{P_{\mu\mu}\left(L_x\right)v}{k_BT} = 1+\frac{B_2^{\mathrm{HS}}\left(d\right)}{v}. \tag{40}$$

On the other hand, if L_x goes to 0, the Eqs. (36)–(37) become

$$\lim_{L_x\to 0}\frac{P_{xx}\left(L_x\right)v}{k_BT} = 1, \tag{41}$$

$$\lim_{L_x\to 0}\frac{P_{\mu\mu}\left(L_x\right)v}{k_BT} = 1+\frac{B_2^{\mathrm{HS}}\left(d-1\right)}{\bar{v}}, \tag{42}$$

where $\bar{v}=v/L_x$ denotes the specific volume projected onto $(d-1)$-dimensional space, v being the d-dimensional specific volume.

Therefore, we find that the parallel component of the pressure tensor of d-dimensional HS fluids confined to the slit pore coincides with that of d and $(d-1)$-dimensional bulk fluids as L_x approaches infinity and 0, respectively, while the orthogonal components of the pressure tensor are given by those of the d-dimensional bulk system and of an ideal gas as L_x goes to infinity and 0, respectively.

III. COMPARISON WITH MOLECULAR DYNAMICS SIMULATION RESULTS

Molecular dynamics (MD) simulations were performed with $N=400$ HS particles with diameter σ and mass m. The number density ρ is defined as N/V and the temperature T is obtained from the average kinetic energy data obeying the equipartition theorem:

$$\frac{d}{2}Nk_BT = \left\langle\frac{1}{2}\sum_{i=1}^{N}m\mathbf{v}_i^2\right\rangle. \tag{43}$$

In our simulations, all physical quantities are given in dimensionless unites by setting k_BT, m, and σ to unity. Accordingly, the time scale is set to unity as $\tau_{\mathrm{MD}}=\sqrt{m\sigma^2\,k_BT}=1$.

We performed MD simulations for $d=2$ and $d=3$ HS fluids at two different densities of $\rho=0.01$ and $\rho=0.1$, and verified the assumption of nonoverlapping exclusion sphere used in deriving the second virial coefficient. Initial particle positions and velocities were taken from uniform and Maxwell–Boltzmann distributions, respectively. The time evolution of the system was calculated via the event-driven MD simulation method.[39,40] Since the particles perform a free motion between subsequent collisions, the equation of motion can be solved exactly up to machine precision, which renders the simulations stable over long periods of time. In order to evaluate the statistical error of each data point, we performed ten independent sets of MD simulations for 500 τ_{MD}.

In the numerical simulations, periodic boundary conditions are applied for all but the x-direction. Two different types of reflective boundary conditions were applied when the particles arrive at $x=\pm L_x/2$. The first strategy is to use a specular wall (S-wall model) which reflects the particle in an elastic way by changing the sign of the velocity component in the x-direction only, and in the second case a Knudsen wall (K-wall model) (Ref. 41) is implemented, which scatters the particles in a random manner, while adjusting the kinetic energy of the scattered particle to the desired kinetic temperature by selecting the velocity of scattered particles from

$$\phi_1(v_x) = \frac{m}{k_BT}|v_x|\exp\left(-\frac{mv_x^2}{2k_BT}\right), \tag{44}$$

$$\phi_2(v_\mu) = \sqrt{\frac{m}{2\pi k_BT}}\exp\left(-\frac{mv_\mu^2}{2k_BT}\right). \tag{45}$$

Downloaded 16 Mar 2011 to 137.250.81.221. Redistribution subject to AIP license or copyright; see http://jcp.aip.org/about/rights_and_permissions

We note that the boundary conditions realized in the S-wall and the K-wall models are two limits of Maxwell's slip boundary condition.[42] The diagonal elements of the pressure component $P_{\alpha\alpha}$ are computed using the virial theorem:

$$P_{\alpha\alpha}V = \left\langle \frac{1}{2}\sum_{i=1}^{N} m\mathbf{v}_i^2 \right\rangle + \frac{1}{\tau}\sum_{c} r_{\alpha,ij}^{(c)}\Delta v_{\alpha,i}^{(c)}, \tag{46}$$

where c denotes summation over all possible collisional events, τ the mean sojourn time between each collision, $r_{\alpha,ij}^{(c)} = r_{\alpha,i}^{(c)} - r_{\alpha,j}^{(c)}$ the α-component of the pairwise distance vector between two particles involved in the collision, and $\Delta v_{\alpha,i}^{(c)}$ the α component of the velocity change of particle i due to such an event.

A. Two-dimensional channel

If $d = 2$, the diagonal components of the pressure tensor shown in Eqs. (34)–(37) are reduced to

$$\frac{P_{xx}v}{k_BT} - 1 = \begin{cases} \dfrac{\sigma^2}{v}\left(\sin^{-1}\dfrac{L_x}{\sigma} - \dfrac{4\sigma}{3L_x}\right), & 0 < L_x < \sigma \\ +E\left(\dfrac{4\sigma^2 - L_x^2}{3v}\right) & \\ \dfrac{\sigma^2}{v}\left(\dfrac{\pi}{2} - \dfrac{4\sigma}{3L_x}\right), & L_x > \sigma \end{cases}, \tag{47}$$

$$\frac{P_{yy}v}{k_BT} - 1 = \begin{cases} \dfrac{\sigma^2}{v}\left(\sin^{-1}\dfrac{L_x}{\sigma} - \dfrac{2\sigma}{3L_x}\right), & 0 < L_x < \sigma \\ +E\left(\dfrac{2\sigma^2 + L_x^2}{3v}\right) & \\ \dfrac{\sigma^2}{v}\left(\dfrac{\pi}{2} - \dfrac{2\sigma}{3L_x}\right), & L_x > \sigma. \end{cases} \tag{48}$$

Therefore, the thermodynamic pressure $P = \left(P_{xx} + P_{yy}\right)/2$ is

$$\frac{Pv}{k_BT} - 1 = \begin{cases} \dfrac{\sigma^2}{v}\left(\sin^{-1}\dfrac{L_x}{\sigma} - \dfrac{\sigma}{L_x} + E\right), & 0 < L_x < \sigma \\ \dfrac{\sigma^2}{v}\left(\dfrac{\pi}{2} - \dfrac{\sigma}{L_x}\right), & L_x > \sigma \end{cases}, \tag{49}$$

where

$$E = \sqrt{\left(\frac{\sigma}{L_x}\right)^2 - 1}. \tag{50}$$

We note that in the region of $0 < L_x < \sigma$, which is generally referred to as the single file regime, the expression of P_{yy} in Eq. (48) is identical to the one obtained from the transfer operator method applied to a canonical isobaric hard disk gas system in the low density region.[27]

Figure 3 compares the components of the diagonal pressure tensor obtained by the MD simulation with the analytical results for various widths L_x. In the low density region [$\rho = 0.01$, Fig. 3(a)], our analytical results in Eqs. (47)–(49) show excellent agreement with the numerical MD simulation results. However for $\rho = 0.1$ [Fig. 3(b)], a non-negligible discrepancy exists between the two results, which tells that our analytical results which contain only up to binary collisions underestimate the pressure compared to the numerical results. It is to be noted that the thermodynamic behavior of confined fluids varies sensitively depending not only on the density ρ, but also on the slit width L_x. For example, the mean interparticle distance of confined fluids in the slit pore increases as L_x when the density is kept at a constant value. Eventually, as L_x goes to 0, the system approaches a $(d-1)$ dimensional ideal gas system even at a finite value of ρ. In order to avoid such an awkward situation occurring in the small L_x regime, we introduce the projected density $\bar{\rho}$ as an effective density parameter in small regions of L_x.

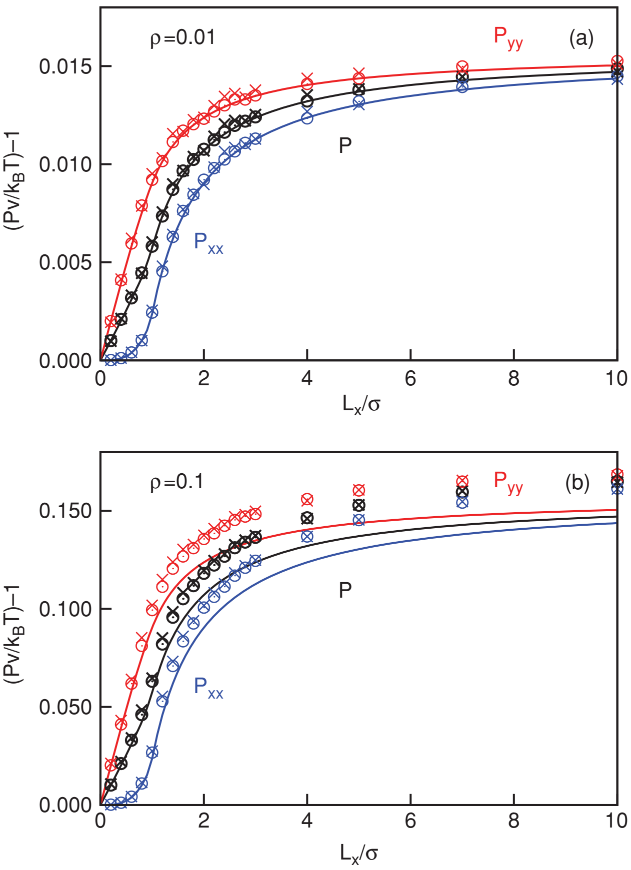

FIG. 3. Diagonal components of the pressure tensor as functions of L_x at number densities (a) $\rho = 0.01$ and (b) $\rho = 0.1$. The analytical results of Eqs. (47)–(49) are displayed as solid lines, and the simulation results are indicated as empty circles (S wall) and crosses (K wall). The statistical error of the simulations is of the order of the symbol size. Each diagonal component is distinguished by a different color: P_{xx}, P_{yy}, and P are colored with blue, red, and black, respectively.

On the other hand, if we increase the size of the slit pore L_x while maintaining the effective density $\bar{\rho}$ at some constant value, the density ρ decreases. Accordingly, the mean interparticle distance increases indefinitely in the large L_x regime, yielding the d-dimensional ideal gas system. In order to properly compare the analytical equations with the numerical results, therefore, we use ρ as a density parameter when we

Downloaded 16 Mar 2011 to 137.250.81.221. Redistribution subject to AIP license or copyright; see http://jcp.aip.org/about/rights_and_permissions

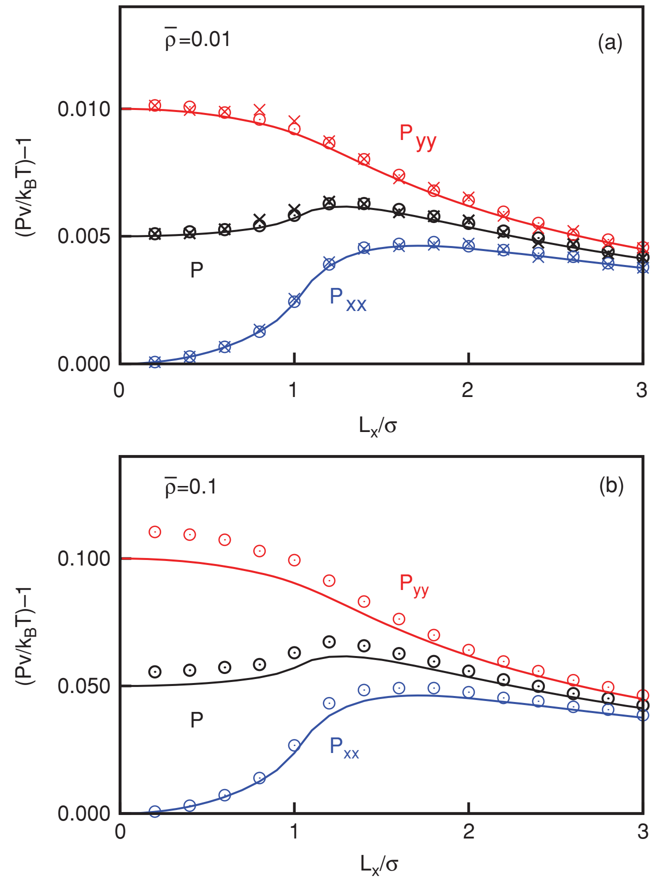

FIG. 4. Dependence of the diagonal components of the pressure tensor as function of the width L_x at constant xy-projected number densities (a) $\bar{\rho} = 0.01$ and (b) $\bar{\rho} = 0.1$. The analytical results of Eqs. (47)–(49) are displayed as solid lines, and the simulation result as empty circles (S wall), and crosses (K wall). The statistical error of the simulations is of the order of the symbol size. Each diagonal component is distinguished by a different color: P_{xx}, P_{yy}, and P are colored with blue, red, and black, respectively.

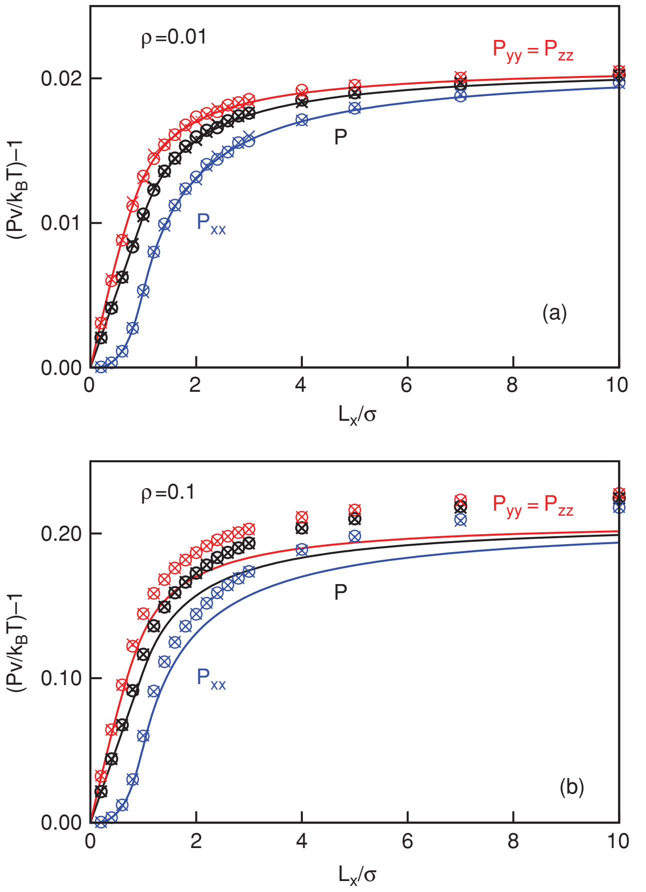

FIG. 5. Diagonal elements of the pressure tensor as a function of L_x for (a) $\rho = 0.01$ and (b) $\rho = 0.1$. The analytical results of Eqs. (51) and (53) are displayed as solid lines, and the simulation results as empty circles (S wall), and crosses (K wall). The statistical error of the simulations is of the order of the symbol size. Each diagonal component is distinguished by different color: P_{xx}, $P_{yy} = P_{zz}$, and P are colored with blue, red, and black, respectively.

investigate the $L_x \to \infty$ regime. On the other hand, we use $\bar{\rho}$ when we investigate $L_x \to 0$ regime.

The behaviors of P, P_{xx}, and P_{yy} as a functions of L_x with $\bar{\rho}$ kept constant are shown in Fig. 4. When $\bar{\rho} = 0.01$ [Fig. 4(a)], our analytical results are in good agreement with the MD simulation results, while in the case of $\bar{\rho} = 0.1$ [see Fig. 4(b)] significant deviations exist between the analytical and MD simulation results due to the considerable contribution of higher virial terms, which are not considered in our analytical treatment.

B. Three-dimensional channel

For $d = 3$, the diagonal components of the pressure tensor in Eqs. (34)–(37) reduce to

$$\frac{P_{xx}v}{k_BT} - 1 = \begin{cases} \dfrac{\pi L_x^3}{6v}, & 0 < L_x < \sigma \\ \dfrac{2\pi\sigma^3}{3v}\left(1 - \dfrac{3\sigma}{4L_x}\right), & L_x > \sigma \end{cases}, \tag{51}$$

$$\frac{P_{yy}v}{k_BT} - 1 = \frac{P_{zz}v}{k_BT} - 1 = \begin{cases} \dfrac{\pi\sigma^2}{2v}L_x\left(1 - \dfrac{L_x^2}{6\sigma^2}\right), & 0 < L_x < \sigma \\ \dfrac{2\pi\sigma^3}{3v}\left(1 - \dfrac{3\sigma}{8L_x}\right), & L_x > \sigma \end{cases}, \tag{52}$$

and the total pressure $P = \left(P_{xx} + P_{yy} + P_{zz}\right)/3$ becomes

$$\frac{Pv}{k_BT} - 1 = \begin{cases} \dfrac{\pi\sigma^2}{3v}L_x, & 0 < L_x < \sigma \\ \dfrac{2\pi\sigma^3}{3v}\left(1 - \dfrac{\sigma}{2L_x}\right), & L_x > \sigma \end{cases}. \tag{53}$$

The analytical and MD simulation results of each diagonal element of the pressure tensor are compared in Fig. 5. At low density [$\rho = 0.01$, Fig. 5(a)], the pressure tensor truncated at the second virial term [Eqs. (51)–(53)] is identical to the numerical MD simulation result within the statistical error. However at the higher density $\rho = 0.1$ [Fig. 5(b)], obviously contributions from higher virial terms become significant.

Downloaded 16 Mar 2011 to 137.250.81.221. Redistribution subject to AIP license or copyright; see http://jcp.aip.org/about/rights_and_permissions

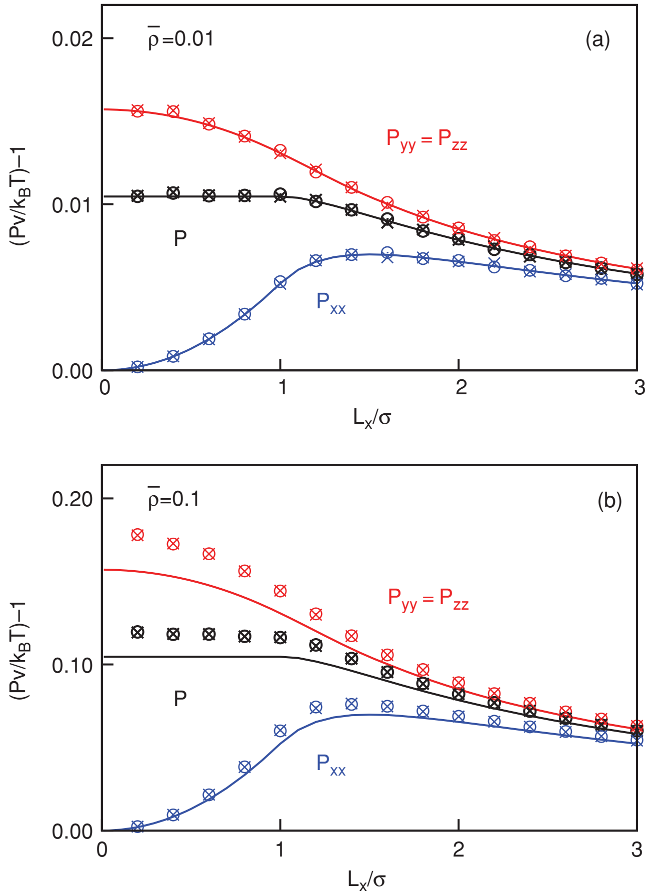

FIG. 6. L_x dependence of the diagonal components of the pressure tensor at constant xy-projected number density (a) $\bar{\rho} = 0.01$ and (b) $\bar{\rho} = 0.1$. The analytical results [Eqs. (51)–(53)] are displayed as solid lines, and the MD simulation results as empty circles (S wall) and crosses (K wall). The statistical error of the simulations is of the order of the symbol size. Each diagonal component is distinguished by a different color: P_{xx}, $P_{yy} = P_{zz}$, and P are colored with blue, red, and black, respectively.

If the projected number density is kept constant at $\bar{\rho} = 0.01$ we found excellent agreement between the analytical and MD simulation results for the pressure tensor as function of L_x. However at the higher density $\bar{\rho} = 0.1$, the pressure components obtained from MD simulations consistently are larger than the analytically obtained values since in the analytical approach virial terms are considered only up to the second order (see Fig. 6).

We found that the contributions of higher order virial terms to the pressure become substantial for $\rho = 0.1$. Figure 7 displays the difference between the pressure, $P^{\text{simul.}}$, obtained by MD simulations, thereby contains all Mayer ring diagrams of the confined HS fluids, and the analytical second order virial approximation, $P^{\text{anal.}}$. When L_x falls below the HS diameter, this suppression becomes most effective. Further, the ring diagrams do not contribute for bulk HS systems in higher dimensions for which higher order correlation functions can be inferred from pair correlation functions and the number density.[43–45] In pore systems, such a decorrelation behavior occurs due to the strong geometric confinement (e.g., see Fig. 8).

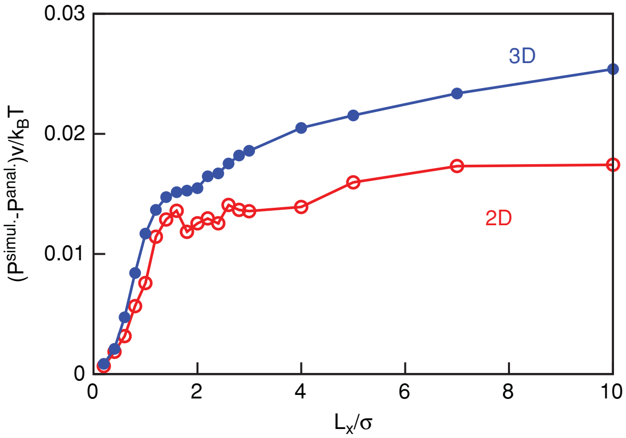

FIG. 7. Differential plot of $P^{\text{simul.}}$ containing all higher virial terms and $P^{\text{anal.}}$ truncated at the second virial term. Contribution of higher order virial terms are suppressed as the pore size decreases, specifically when L_x is smaller than than the order of σ.

Another important point to be addressed here is that the thermodynamic behavior of a confined fluid does not depend on the type of the wall boundary condition. As demonstrated in Figs. 3 and 6, the MD simulation results of the diagonal elements of the pressure tensor obtained for different wall conditions perfectly agree for all widths L_x and densities. Further it implies that the EOS of a confined fluid depends only on the geometry of the free volume but not on the wall boundary condition. This means that thermodynamic properties can be interpreted in terms of statistical geometry even in the case of confined fluids. This is unlike the case of transport properties, since in this case, the diffusion behavior sensitively depends on the type of particle reflection at a wall.[30]

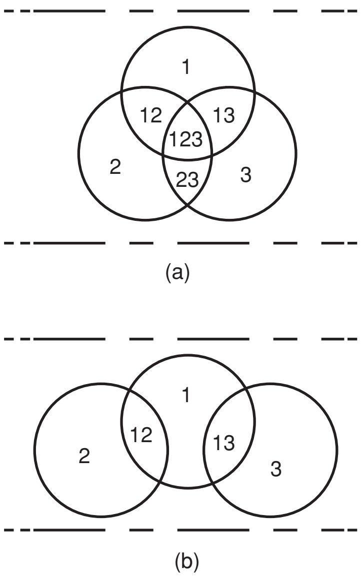

FIG. 8. Higher order correlations are decoupled into pair correlations. Triplet correlation is shown as an example. (a) When $L_x > \sigma$, there can be a subvolume of three exclusion spheres (v_{123}). (b) When $L_x < \sigma$, no subvolume of three exclusion spheres is allowed ($v_{123} = 0$).

Downloaded 16 Mar 2011 to 137.250.81.221. Redistribution subject to AIP license or copyright; see http://jcp.aip.org/about/rights_and_permissions

IV. CONCLUSION

In the present work, we derived the second virial coefficient B_2 of d-dimensional HS fluids confined to the slit pore composed of two parallel $(d-1)$-dimensional hyperplanes.

The calculation of the second virial coefficient B_2 was performed using two different methods. The first method generalizes the free volume concept developed for bulk HS fluid system to d-dimensional HS fluid systems confined to slit pores.[35] The second method is an extension of Mukamel and Posch's method[28] which is based on the Mayer cluster expansion. These two methods produce exactly the same results for the second virial coefficient B_2, even though they are based on the evaluation of different geometrical factors; the first method uses the surface area and the second one the volume of exclusion spheres.

From the virial coefficient B_2, an analytical form of the free energy and of the diagonal components of the pressure tensor, as well as the EOS of HS fluids confined to slit pores were obtained.

MD simulations were performed for HS fluids confined to slit pores, and the EOS was evaluated for both $d = 2$ and $d = 3$ dimensional cases to examine to what extent the analytical results reliably reflect the thermodynamic behavior. For $\rho = 0.1$, in the high density regime, the agreement between the analytical and MD simulation results becomes better as the width of the slit pore decreases. This is due to the suppression of the contribution of higher virial terms to the EOS.

Lastly, we showed that equilibrium thermodynamic properties of confined HS fluids are insensitive to the implemented wall boundary condition. This is an interesting result, since it tells us that even in the case of confined fluids, the statistical thermodynamic problems can be successfully transformed to statistical geometric problems.

ACKNOWLEDGMENTS

This work was supported by the German Excellence Initiative via *Nanosystems Initiative Munich* (NIM), by the Deutsche Forschungsgemeinschaft under the Grant No. HA 1517/25-2, by the Basic Science Research Program through the National Research Foundation of Korea (NRF) funded by the Ministry of Education, Science, and Technology (MEST) (Grant No. 2010-0013812), and by the World Class University programs through NRF funded by the MEST (Grant No. R31-2008-000-10055-0).

APPENDIX A: CALCULATION OF $S(a)$ AND $V(a)$

The calculation of a volume and a surface area of a hypersphere trimmed by a plane wall (i.e., cropped sphere) is a key step in the evaluation of B_2. We consider the d-dimensional hypersphere defined by $x^2 + y^2 + z^2 + \cdots = \sigma^2$ cropped by a wall located at $x = a$ as shown in Fig. 9 ($a \in [0, \sigma]$). We denote the volume and the surface area of the hypersphere when $x < a$ by $V(a)$ and $S(a)$, respectively. Since for $a \geq \sigma$, $V(a)$ and $S(a)$ simply are the volume and the surface area of an entire hypersphere, here we only consider the case $a < \sigma$. In the d-dimensonal hyperspherical coordinate system, the volume element is defined as

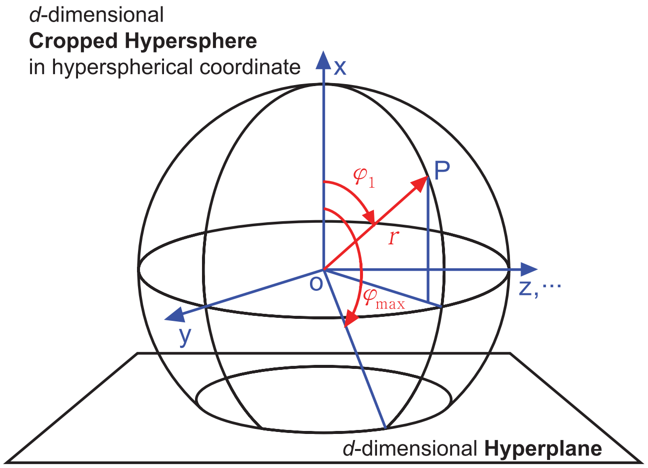

FIG. 9. Hyperspherical coordinates in the d-dimensional space are depicted. The azimuthal angle φ_1 is defined as the vertical angle from the axis passing through the center of the sphere (chosen as x-direction). The azimuth angle φ_1 is restricted to $[0, \varphi_{\max}]$, where $\varphi_{\max} = \cos^{-1}(-a/\sigma)$.

$$d_{\mathbb{R}^d} V = \left| \det \frac{\partial(x_i)}{\partial(r, \varphi_j)} \right| dr d\varphi_1 d\varphi_2 \cdots d\varphi_{d-1}, \tag{A1}$$

where r is the radial coordinate and φ_i's are the angle coordinates. Without loss of generality we took φ_1 as the azimuthal angle from the x-axis shown in Fig. 9. Due to the cropped geometry of the hypersphere, φ_1 ranges from 0 to $\varphi_{\max} = \cos^{-1}(-a/\sigma)$. If we integrate out the remaining angles $\varphi_2, \cdots, \varphi_{d-2}$, and φ_{d-1}, we obtain

$$\begin{aligned} dV &= \int_{\varphi_2=0}^{\pi} \cdots \int_{\varphi_{d-2}=0}^{\pi} \int_{\varphi_{d-1}=0}^{2\pi} d_{\mathbb{R}^d} V \\ &= \frac{(d-1)\pi^{\frac{d-1}{2}}}{\Gamma((d+1)/2)} \sin^{d-2}\varphi_1 \, r^{d-1} \, dr \, d\varphi_1 \end{aligned} \tag{A2}$$

and

$$dS = \frac{(d-1)\pi^{\frac{d-1}{2}}}{\Gamma((d+1)/2)} \sin^{d-2}\varphi_1 \, \sigma^{d-1} \, d\varphi_1. \tag{A3}$$

This yields the volume and the surface area of the cropped hypersphere as a function of a:

$$\begin{aligned} V(a) &= \int_0^{\pi} \int_0^{\sigma} dV - \int_{\varphi_{\max}}^{\pi} \int_{\frac{a}{\cos(\pi-\varphi_1)}}^{\sigma} dV \\ &= C \frac{(d-1)}{\sigma} \left[F^{(\mathrm{I})}(1) + \frac{a}{\sigma} F^{(\mathrm{I})}\left(\frac{a^2}{\sigma^2}\right) + A \right] \end{aligned} \tag{A4}$$

and

$$\begin{aligned} S(a) &= \int_0^{\varphi_{\max}} dS \\ &= C \frac{d(d-1)}{\sigma} \left[F^{(\mathrm{I})}(1) + \frac{a}{\sigma} F^{(\mathrm{I})}\left(\frac{a^2}{\sigma^2}\right) \right], \end{aligned} \tag{A5}$$

where $F^{(\mathrm{I})}$ and C are previously defined in Eqs. (14)–(13), respectively.

Downloaded 16 Mar 2011 to 137.250.81.221. Redistribution subject to AIP license or copyright; see http://jcp.aip.org/about/rights_and_permissions

APPENDIX B: WHEN A PARTICLE IS CONFINED TO A CHANNEL SATISFYING PERIODIC BOUNDARY CONDITIONS

When the HS particles are confined to a narrow channel satisfying PBC, the *exclusion sphere* has an overlap with its image for $0 < L_x < 2\sigma$, and otherwise, it is a full hypersphere. Therefore, $\langle S_{\mathrm{ExS}} \rangle$ and $\langle V_{\mathrm{ExS}} \rangle$ are given as

$$\langle S_{\mathrm{ExS}} \rangle = \begin{cases} 2S\left(\dfrac{L_x}{2}\right) - S(\sigma), & 0 < L_x < 2\sigma \\ S(\sigma), & L_x \geq 2\sigma \end{cases}, \tag{B1}$$

$$\langle V_{\mathrm{ExS}} \rangle = \begin{cases} 2V\left(\dfrac{L_x}{2}\right) - V(\sigma), & 0 < L_x < \sigma \\ V(\sigma), & L_x \geq \sigma \end{cases}. \tag{B2}$$

Substitutions of Eqs. (12) and (25) into Eqs. (B1) and (B2) produce $\langle S_{\mathrm{ExS}} \rangle$ and $\langle V_{\mathrm{ExS}} \rangle$, respectively. Then we obtain B_2 either by using Eq. (6) or by using Eq. (22), which is identical to each other:

if $0 < L_x < 2\sigma$,

$$B_2 = \frac{d-1}{2\sigma^2} C L_x F^{(1)}\left(\frac{L_x^2}{4\sigma^2}\right), \tag{B3}$$

if $L_x \geq 2\sigma$,

$$B_2 = B_2^{\mathrm{HS}}(d). \tag{B4}$$

Thus, it shows that Eq. (1) is also applicable for the evaluation of the EOS of d-dimensional HS confined to a channel satisfying PBC.

For $d = 2$, Eqs. (B3) and (B4) becomes

$$B_2 = \begin{cases} \sigma^2 \sin^{-1}\left(\dfrac{L_x}{2\sigma}\right), & 0 < L_x < \sigma \\ \dfrac{1}{2}\pi\sigma^2, & L_x > \sigma \end{cases}. \tag{B5}$$

This recovers the previous result of Mukamel and Posch, which was already numerically confirmed.[28]

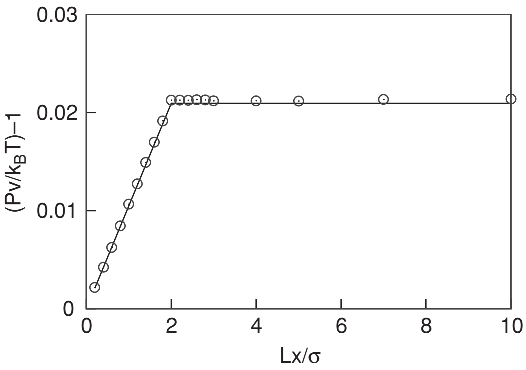

FIG. 10. Compressibility factor of 3D HS fluids as a function of L_x for $\rho = 0.01$. The boundary condition of the pore is periodic. The analytical result of Eq. (B6) is displayed as a solid line, and the simulation results as empty circles. The statistical error of the simulations is of the order of the symbol size.

For $d = 3$, Eqs. (B3) and (B4) becomes

$$B_2 = \begin{cases} \dfrac{1}{3}\pi\sigma^2 L_x, & 0 < L_x < \sigma \\ \dfrac{2}{3}\pi\sigma^3, & L_x > \sigma \end{cases}. \tag{B6}$$

We performed MD simulations of 3D HS fluids in a channel with PBC for $\rho = 0.01$, which yield perfect agreement with then analytical result of Eq. (B6) as shown in shown in Fig. 10.

[1] F. Gambale, M. Bregante, F. Stragapede, and A. M. Cantu, J. Membr. Biol. **154**, 69 (1996).
[2] Z. Siwy, I. D. Kosińska, A. Fuliński, and C. R. Martin, Phys. Rev. Lett. **94**, 048102 (2005).
[3] D. Reguera, G. Schmid, P. S. Burada, J. M. Rubi, P. Reimann, and P. Hänggi, Phys. Rev. Lett. **96**, 130603 (2006).
[4] B. J. Hinds, N. Chopra, T. Rantell, R. Andrews, V. Gavalas, and L. G. Bachas, Science **303**, 62 (2004).
[5] K. Hahn, J. Kärger, and V. Kukla, Phys. Rev. Lett. **76**, 2762 (1996).
[6] V. Gupta, S. S. Nivarthi, D. Keffer, A. V. McCormick, and H. T. Davis, Science **274**, 164 (1996).
[7] C. T. Kresge, M. E. Leonowicz, W. J. Roth, J. C. Vartuli, and J. S. Beck, Nature (London) **359**, 710 (1992).
[8] M. E. Davis, Nature (London) **417**, 813 (2002).
[9] A. Katz and M. E. Davis, Nature (London) **403**, 286 (2000).
[10] P. S. Burada, P. Hänggi, F. Marchesoni, G. Schmid, and P. Talkner, Chem. Phys. Chem **10**, 45 (2009).
[11] S. S. Han and W. A. Goddard, J. Am. Chem. Soc. **129**, 8422 (2007).
[12] S. S. Han, W.-Q. Deng, and W. A. Goddard, Angew. Chem., Int. Ed. **46**, 6289 (2007).
[13] S. S. Han, H. Furukawa, O. M. Yaghi, and W. A. Goddard, J. Am. Chem. Soc. **130**, 11580 (2008).
[14] S. S. Han and W. A. Goddard, J. Phys. Chem. C **112**, 13431 (2008).
[15] S. S. Han, J. L. Mendoza-Cortes, and W. A. Goddard, Chem. Soc. Rev. **38**, 1460 (2009).
[16] B. C. H. Steele and A. Heinzel, Nature (London) **414**, 345 (2001).
[17] L. Carrette, K. A. Friedrich, and U. Stimming, Chem. Phys. Chem **1**, 162 (2000).
[18] K. D. Kreuer, J. Membr. Sci. **185**, 29 (2001).
[19] S. J. Paddison, Annu. Rev. Mater. Res. **33**, 289 (2003).
[20] Q. F. Li, R. H. He, J. O. Jensen, and N. J. Bjerrum, Chem. Mater. **15**, 4896 (2003).
[21] K. A. Mauritz and R. B. Moore, Chem. Rev. **104**, 4535 (2004).
[22] M. A. Hickner and B. S. Pivovar, Fuel Cells **5**, 213 (2005).
[23] H. Kim, W.-Q. Deng, W. A. Goddard, S. S. Jang, M. E. Davis, and Y. Yan, J. Phys. Chem. C **113**, 819 (2009).
[24] Q. S. Xin, I. Hiyane, and P. Siders, J. Chem. Soc., Faraday Trans. **90**, 973 (1994).
[25] E. D. Glandt, AIChE J. **27**, 51 (1981).
[26] A. J. Post and D. A. Kofke, Phys. Rev. A **45**, 939 (1992).
[27] I. E. Kamenetskiy, K. K. Mon, and J. K. Percus, J. Chem. Phys. **121**, 7355 (2004).
[28] D. Mukamel and H. A. Posch, J. Stat. Mech.: Theory Exp. P03014 (2009).
[29] H. Kim, C. H. Cho, and E. K. Lee, J. Theor. Comput. Chem. **4**, 305 (2005).
[30] H. Kim, C. Kim, E. K. Lee, P. Talkner, and P. Hänggi, Phys. Rev. E **77**, 031202 (2008).
[31] N. F. Carnahan and K. E. Starling, J. Chem. Phys. **51**, 635 (1969).
[32] N. F. Carnahan and K. E. Starling, J. Chem. Phys. **53**, 600 (1970).
[33] W. G. Hoover, W. T. Ashurst, and R. Grover, J. Chem. Phys. **57**, 1259 (1972).
[34] W. G. Hoover, N. E. Hoover, and K. Hanson, J. Chem. Phys. **70**, 1837 (1979).
[35] R. J. Speedy, J. Chem. Soc., Faraday Trans. 2 **76**, 693 (1980).
[36] R. J. Speedy and H. Reiss, Mol. Phys. **72**, 999 (1991).
[37] S. Sastry, D. S. Corti, P. G. Debenedetti, and F. H. Stillinger, Phys. Rev. E **56**, 5524 (1997).
[38] S. Sastry, T. M. Truskett, P. G. Debenedetti, S. Torquato, and F. H. Stillinger, Mol. Phys. **95**, 289 (1998).

Downloaded 16 Mar 2011 to 137.250.81.221. Redistribution subject to AIP license or copyright; see http://jcp.aip.org/about/rights_and_permissions

[39] D. C. Rapaport, *The Art of Molecular Dynamics Simulation* (Cambridge University Press, Cambridge, England, 2001).

[40] M. P. Allen and D. J. Tildesley, *Computer Simulation of Liquids* (Oxford University Press, Oxford, New York, 1991).

[41] M. Knudsen, Ann. Phys. **333**, 75 (1909).

[42] J. C. Maxwell, Philos. Trans. R. Soc. London **170**, 231 (1879).

[43] H. L. Frisch and J. K. Percus, Phys. Rev. E **60**, 2942 (1999).

[44] S. Torquato and F. H. Stillinger, Exp. Math. **15**, 307 (2006).

[45] S. Torquato and F. H. Stillinger, Phys. Rev. E **73**, 031106 (2006).

Downloaded 16 Mar 2011 to 137.250.81.221. Redistribution subject to AIP license or copyright; see http://jcp.aip.org/about/rights_and_permissions